EPJ preprint
(published in EPJ ST, doi:10.1140/epjs/s11734-022-00701-8)

Difference Recurrence Plots for Structural Inspection Using Guided Ultrasonic Waves

A New Approach for Evaluation of Small Signal Differences

Carsten Brandt[1,a] and Norbert Marwan[2]

[1] Private Researcher, Bremen, Germany
[2] Potsdam Institute for Climate Impact Research (PIK), Member of the Leibniz Association, Telegrafenberg A31, 14473 Potsdam, Germany

Abstract. We propose a novel recurrence plot based approach, the difference recurrence plot (DRP), to detect small deviations between measurements. By using a prototypical model system, we demonstrate the potential of DRPs and the difference to alternative measures, such as Pearson correlation, spectral analysis, or cross and joint recurrence analysis. Real world data comes from an application of guided ultrasonic waves for structural health monitoring to detect damages in a composite plate. The specific challenge for this damage detection is to differentiate between defects and the influence of temperature. We show that DRPs are suited in the following sense: DRPs of two time series that derive from measurements at different temperatures hold practically full recurrence, whereas DRPs of one time series from a measurement without and one time series with defect show a hugely reduced recurrence rate.

1 Introduction

The rise of advanced data analytics and machine learning, being enabled by increased computational power and memory, and data availability, has had its effect on non-destructive testing (NDT) as well as on structural health monitoring (SHM). Both NDT and SHM are used to find defects in materials, and sophisticated evaluation methods help to improve detection capabilities, for example to find smaller cracks in metals. NDT uses probes and equipment separate from the inspected part; SHM uses, instead, permanently installed sensors on the inspected part, with interrogation either during use or when not in use of, e.g., a craft.

Acousto-ultrasonics is an SHM method using a grid of acoustic sensors (piezos) for example on a fuselage shell, which both send and receive guided ultrasonic waves, mechanical waves that propagate along the elongated dimension of the inspected part [1]. When inspecting composite parts (e.g., carbon fibre reinforced polymers, CFRP), guided ultrasonic waves are disturbed by delaminations, material separations within the material (caused by, e.g., hail or bird strike), so that such defects can be detected.

[a] e-mail: carsten.brandt@uni-bremen.de

When applied during use of, e.g., an aircraft, the following challenge arises: environmental changes, especially different temperatures, have a large effect on the signal, too, so that the effect of defects might be masked. One approach to overcome this is the so-called continuous baseline update: measurements are taken every x minutes, and assuming that only small temperature changes take place during this interval, the effect of a defect exceeds the one of the changed temperature.

Typical evaluation bases on a comparison of two consecutive measurements. The differences between these two time series are small compared to the signal amplitudes. Instead of the usually asked research question to detect whether two signals from different sources are correlated or synchronised, we are here interested in detecting small deviations from originally identical signals. To be exact: for the application we are going to describe, we always have small differences between time series, and we are interested in detecting differences in these differences (i.e., distinguishing between only temperature differences between the measurements that create these time series or temperature differences plus an appearing defect).

We propose a new method for evaluation of two time series with very small signal differences, the difference recurrence plot (DRP), firstly proposed in [2] and rooted in recurrence quantification analysis (RQA).

2 Structural Health Monitoring with Guided Ultrasonic Waves

Structural health monitoring (SHM) aims at checking the structural integrity, especially the occurrence of defects, with permanently installed sensors. Acousto-ultrasonics use guided ultrasonic waves; the latter are mechanical waves above the audible range (20 kHz) that propagate along the elongated dimensions of the inspected part. The waves are sent and received with piezo transducers, which have to cover the surface of, e.g., a composite plate in a grid like manner.

Guided ultrasonic waves can be used for example to detect damages in composite structures, e.g., after impact (through birds, hail etc.). Such damages influence the propagation of the waves and, thus, can be detected using acousto-ultrasonics. A challenge for the use of guided ultrasonic waves is however the effect of environmental conditions, especially temperature. If an SHM system using guided waves shall operate during use of, e.g., an aircraft, temperature changes might hide effects on the received guided wave that are caused by impact damages. Different methods exist to overcome this challenge (see [3] for an overview). One approach is the continuous baseline update: throughout the operation of an aircraft, measurements are taken after rather short intervals, in the range of several minutes. Each measurement is compared with the former measurement, which serves as baseline. If only small changes occur, this is expected to be related to temperature, and the current measurement becomes the new baseline. Impact damages are supposed to cause relatively great changes between the current measurement (time series) and the former one. Such relatively great changes thus indicate damages; the current measurement cannot serve as baseline.

Means of time series analysis to differentiate between small changes due to temperature and slightly larger changes due to a damage have to be found to deploy continuous baseline update. In terms of data evaluation and time series analysis there are two different approaches to do so: either features of each time series are computed and compared to each other, as done in [3] with some standard features as well as with recurrence rate (RR) of standard (univariate) recurrence plots (RPs); or bivariate time series analysis is deployed to compare the former measurement (the baseline) and the current measurement with each other. We describe the latter in Sect. 4 utilising difference recurrence plots (DRPs) for this application.

3 Recurrence Based Difference Analysis

Differences (or similarities) between time series can be detected using linear and nonlinear methods, such as correlation coefficients, comparing power and wavelet spectra, mutual information, or using recurrences. Recurrence based methods have been shown to be versatile tools for detecting various phenomena related to differences or similarties between time series or dynamical systems, such as time scale differences [4], phase synchronisation [5], nonlinear [6] and hidden couplings [7], or even coupling directions [8]. Moreover, RPs have been shown to be very sensitive on very small changes such as frequency modulations, where other methods fail [9, 10].

The two main extensions of RPs for direct comparison of recurrence features are cross and joint RPs. A cross recurrence plot (CRP) identifies differences between the phase space trajectories $\vec{x}_i$ and $\vec{y}_i$ of system X and system Y by [11]

$$CR_{i,j} = \Theta\big(\varepsilon - D_{i,j}(X,Y)\big), \tag{1}$$

with $D_{i,j}(X,Y) = \|\vec{x}_i - \vec{y}_j\|$ the Euclidean distance between the states $\vec{x}_i$ and $\vec{y}_i$ in phase space, Θ the Heaviside function, and ε the recurrence threshold [12]. Large deviations in the phase space trajectories result in missing recurrences. But the main potential of CRPs is their ability to extract slight temporal differences in mostly identical system (where some time distortions were applied) in a non-parametric way [13, 14]. For a CRP based similarity analysis, we can simply use the average number of recurrence points on the main diagonal (the τ-(cross) recurrence rate at lag 0, [4]), $cRR_0 = \frac{1}{N}\sum_{i=1}^{N} CR_{i,i}$ (with N the length of the time series or the number of phase space vectors), which would be $cRR_0 = 1$ for identical systems and $cRR_0 \to 0$ for non-identical systems.

In contrast, the joint recurrence plot (JRP) compares the differences in the individual recurrence pattern, represented by the element-wise multiplication of the individual RPs [6]

$$JR_{i,j} = \Theta\Big(\varepsilon - \big\|D_{i,j}(X,X)\big\|\Big) \cdot \Theta\Big(\varepsilon - \big\|D_{i,j}(Y,Y)\big\|\Big), \tag{2}$$

where $D_{i,j}(X,X) = \|\vec{x}_i - \vec{x}_j\|$ is the distance matrix of the pairwise Euclidean distances of all states in system X (and analogous for system Y). Thus, the focus is on identifying simultaneous recurrences. Using JRPs, we can define measures for generalised synchronisation or nonlinear couplings [6, 15]. Here, we use the average joint probability of recurrence [5],

$$p_{\mathrm{JR}} = \frac{\frac{1}{RR \cdot N^2}\sum_{i,j=1}^{N} JR_{i,j} - RR}{1 - RR}, \tag{3}$$

where we ensure the same recurrence rate $RR = \frac{1}{N^2}\sum_{i,j=1}^{N} R_{i,j}$ for X and Y by selecting appropriate values for the recurrence threshold ε [12]. We expect $p_{\mathrm{JR}} = 1$ for systems with identical recurrence structure and $p_{\mathrm{JR}} \to 0$ for systems with diverging recurrence structure.

Both approaches complement each other and work very well for different research questions in various scientific disciplines, such as measuring the coordination between communicating people [16], detecting the coupling structure within the cardio-respiratory [17] or the climate system [18, 19], studying the asynchrony between photovoltaic power generation and solar irradiance [20] or between the north-south sunspot activity [14], or assessing the synchronisation between ecological components or multi-species communities [21, 22].

In specific applications, such as NDT and SHM, the identification of tiny deviations in the amplitude of signals is important. Standard methods, such as Pearson correlation or spectral methods, are usually not sensitive enough to reveal a significant result.

Therefore, we propose a new recurrence based measure which is based on the difference of the individual distance matrices $\mathbf{D}(X, X)$ and $\mathbf{D}(Y, Y)$ [2]. The difference $\mathbf{D}(X, X) - \mathbf{D}(Y, Y)$ contains all deviations in the geometry of the phase space trajectories, not only in the neighbourhoods, but also for the state relationship of far away states. By thresholding these differences, we can define a quantifier, similar to standard RPs:

$$DR_{i,j} = \Theta\Big(\varepsilon - \big|D_{i,j}(X, X) - D_{i,j}(Y, Y)\big|\Big). \tag{4}$$

This difference RP (DRP) represents all pairs of states which do not deviate with respect to a small error ε. The sensitivity of the detected deviations can be controlled by the selection of the threshold ε. Using the same approach as for the RPs (fixing the threshold to ensure a predefined RR of, e.g., $RR = 0.05$) would not make much sense, because the idea is the use the RR ($RR_{\mathrm{DR}} = \frac{1}{N^2}\sum_{i,j=1}^{N} DR_{i,j}$) of the DRP for detecting deviations. Therefore, the threshold selection procedure has to be selected corresponding to the research question. According to our experience and many numerical experiments, to set ε to a fixed value corresponding to 0.1% of the standard deviation of the original (reference) signal u_1 works well in most cases. For our specific research question of SHM, we will select a larger ε in order to get the differences caused by structural changes and not by temperature (procedure explained below).

We illustrate this approach by comparing the z-component of the Lorenz system

$$\begin{aligned} \frac{dx}{dt} &= 10(y - x), \\ \frac{dy}{dt} &= 28x - y - xz, \\ \frac{dz}{dt} &= -\frac{8}{3}z + xy, \end{aligned} \tag{5}$$

with an almost identical copy of it which has a very small deviation in the amplitude. The ODE is integrated using a Runge-Kutte schema (4^{rd} order) for $10,000$ time points with final temporal sampling of $\Delta t = 0.005\,\mathrm{s}$ and removing the first $5,000$ data points as transients (final length $N = 5,000$). Using $z(t)$ we define two almost identical time series U_1 and U_2 (Fig. 1) by

$$\begin{aligned} u_1(t) &= z(t), \\ u_2(t) &= z(t) + 0.1\sin(0.4 \cdot 2\pi t) \end{aligned} \tag{6}$$

and compare them by Pearson correlation, power spectra, wavelet analysis, CRP, JRP, and DRP.

The Pearson correlation between both time series is $\varrho = 1.000$, indicating the very high similarity between the two time series U_1 and U_2. The power spectrum as well as the wavelet spectrum show also very similar results for both U_1 and U_2 (Figs. 2 and 3).

Using RP based methods, we use the CRP to find differences between the states of two systems (i.e., amplitude differences) and the JRP to measure simultaneuous recurrences. The individual RPs (calculated with embedding dimension $m = 3$, delay $\tau = 37\Delta t$, and recurrence threshold ε selected to ensure a fixed RR of $RR = 0.05$) appear to be almost identical (Fig. 4A, B). For the CRP based similarity analysis (same parameters used as for the individual RPs), we use cRR_0; for JRP based

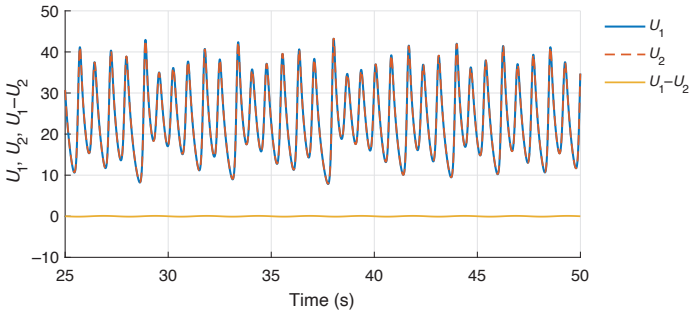

Fig. 1. Almost identical time series U_1 and U_2 based on the z-component of the Lorenz system.

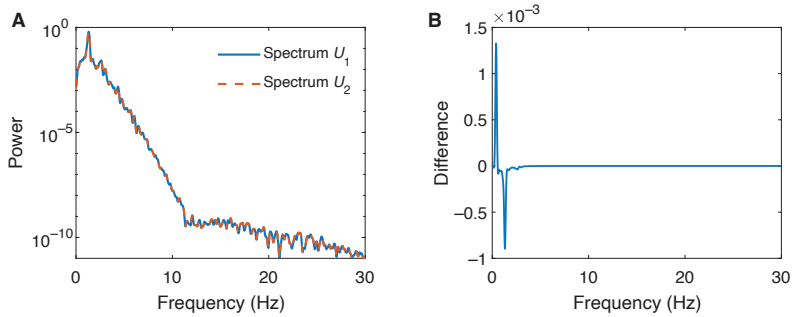

Fig. 2. (A) Power spectra of very similar signals U_1 and U_2 and (B) their difference, indicating their strong similarity in the frequency domain.

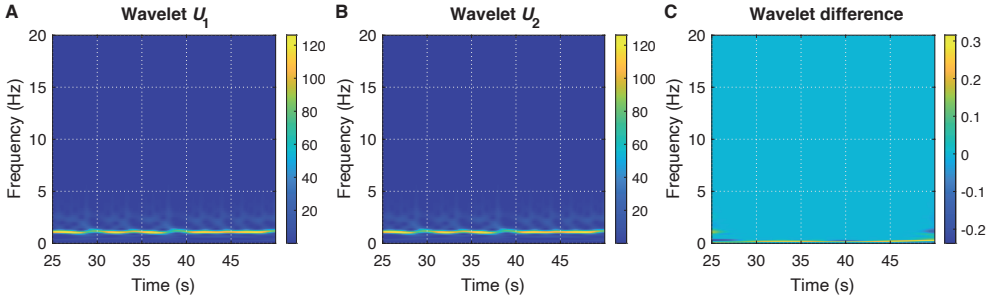

Fig. 3. (A, B) Wavelet analysis of very similar signals U_1 and U_2 and (C) their difference, indicating their strong similarity in the time-frequency domain.

comparison, we use the average joint probability of recurrence p_{JR}. For CRP, we find $cRR_0 = 1.00$, indicating identical time series U_1 and U_2, although their amplitudes actually differ slightly; for JRP, we find $p_{\mathrm{JR}} = 0.985$, indicating only a very small deviation in the recurrence structure (Fig. 4C, D).

The matrix with the differences between the distance matrices $\left|\mathbf{D}(U_1, U_1) - \mathbf{D}(U_2, U_2)\right|$ reveals the pair-wise distribution of these differences in terms of absolute values (Fig. 5A). By thresholding this matrix, Eq. (4), using 0.1% of the standard deviation of U_1 we can identify the specific pattern of those pairs of states where the amplitude deviations vanish (Fig. 5B). In the selected example, we added periodic distortions which are now clearly visible by the periodic structures in this DRP (with period length of 2.5 s, corresponding to the frequency of the distorting signal of 0.4,

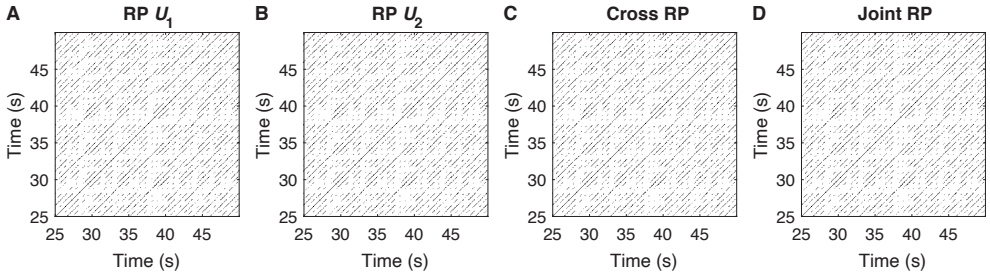

Fig. 4. (A, B) Recurrence plots of very similar signals U_1 and U_2, (C) cross and (D) joint recurrence plot between U_1 and U_2, indicating the strong coincidence in the phase space and the recurrence patterns.

Eq. (6)). The resulting RR is $RR_{\mathrm{DR}} = 0.124$, i.e., less than 13% of all pairs do not deviate with respect to the neighbourhood relationship in the phase space.

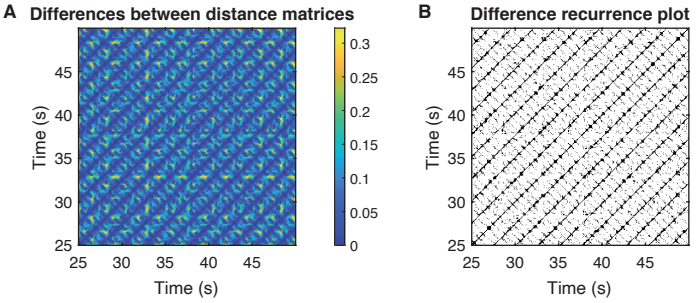

Fig. 5. (A) Difference matrix $|\mathbf{D}(U_1, U_1) - \mathbf{D}(U_2, U_2)|$ and (B) difference recurrence plot. Both plots are characterised by a periodic pattern related to the periodic nature of the distortion signal.

Next, we consider a continuous increase of the distorting signal, ensuring a continuous difference of U_2 from U_1 by increasing the deviation coefficient α from 0 to 1.5 in $u_2(t) = z(t) + \alpha \sin(0.4 \cdot 2\pi t)$. Pearson correlation and the CRP based measure cRR_0 are not able to identify the differences in this range of α (Fig. 6). The JRP based measure is slowly monotonously decreasing, pointing to the increasing difference between U_1 and U_2. But only the RR of the DRP identifies quickly the tiny difference (Fig. 6). This result is robust for different (small) values of the recurrence threshold ε. For very small $\varepsilon = 0.1\%$ of the signal's standard deviation, the smallest difference resulting from small α can be identified.

Standard measures are usually designed to detect interrelationships, coupling, or synchronisation. Therefore, they are sensitive against the null-hypothesis that the systems are not linked to each other, thus, are less sensitive for detecting small deviations or differences between the signals. In contrast, the novel approach of DRP is designed to be sensitive for such small deviations and is, therefore, outperforming the standard measures considered here. The usefulness of the DRP approach is limited to such research questions where we are sure to have identical or very similar (strongly coupled) systems or dynamics and are interested in the deviations. It would not make much sense to apply it for noisy data. In the following, we will demonstrate the use of this novel approach of detecting small deviations between different data sets for the practical application in SHM.

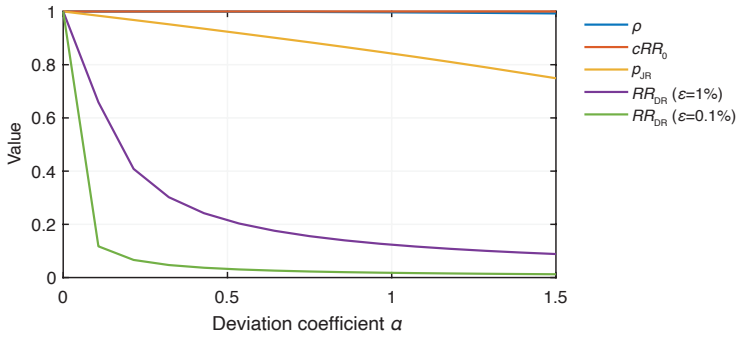

Fig. 6. Measures of "deviation" (Pearson correlation ϱ, CRP based cRR_0, JRP based p_{JR}, and DRP based RR_{DR} for two different recurrence thresholds ε) between U_1 and U_2 for increasing deviation in signal U_2.

4 Application of Difference Recurrence Plots on Ultrasonic Guided Wave Data

We use publicly available data of guided ultrasonic waves on a plate of a composite material (CFRP, carbon fibre reinforced polymer), with reversible damages available on [23], cf. [24, 25]. The specificities of these data are:

- Taken on an approximately 0.5 m × 0.5 m CFRP plate with two rows, each of six piezo transducers, one at the top and one at the bottom of the plate (cf. Fig. 7 with the four transducers used in this paper),
- Each transducer sent once and all transducers receive (except for double paths — sending and receiving is interchangeable),
- Guided ultrasonic waves with mean frequencies between 40 kHz and 260 kHz (in 20 kHz steps),
- Signals digitised with 10 MHz,
- Measurements were taken at varying temperatures changes, ascending and descending between ≈ 20 °C and ≈ 60 °C (Fig. 8) in ≈ 0.5 K steps,
- Measurements with varying temperatures were taken without and with four different reversible damages (represented by an aluminium disc temporarily fixed on the surface of the plate by tacky tape).
- Measurement time series are 1.3 ms long, thus 13,000 data point.
  In this paper (as in [3]) we use the portion from 0.3 ms up to the end, 1.3 ms. Processed time series are thus 1 ms, 10,000 data points long.

4.1 Evaluation goals and RQA parameter determination (training)

The goal of our investigations of difference recurrence plots (DRPs) for the continuous baseline update of guided ultrasonic waves is to find features that provide great changes between time series if a defect appears and only small changes for (small) temperature changes (c.f. Sect. 2). The available data contains measurement series at varying temperatures without and measurement series at varying temperatures with defects. Our approach based on these data is as follows:

- We decided that 5 K temperature steps (cf. dots in Fig. 8) represent temperature steps that may occur in potential later use when measuring every x minutes during use of, e.g., an aircraft.

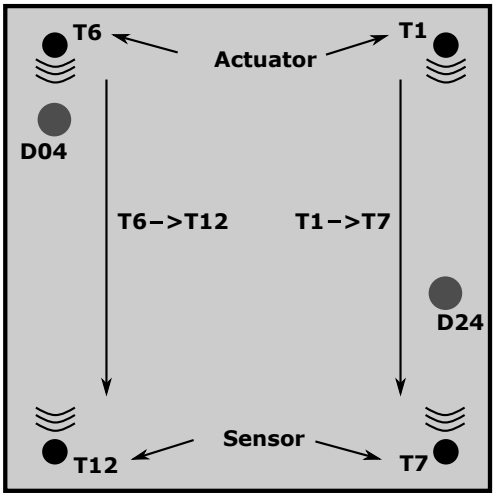

Fig. 7. Specimen with transducers, sound paths and defects used for training, i.e., RQA parameter determination (T1 – T7, defect D24, right hand side) and test, i.e., evaluation (T6 – T12, defect D04, left hand side).

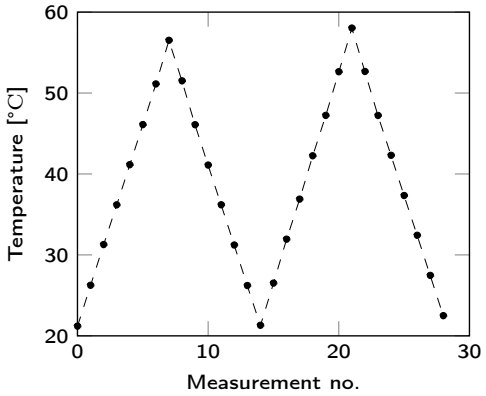

Fig. 8. Course of temperatures for guided ultrasonic wave measurements in [23]; dots represent the temperature values of measurements evaluated in this paper.

- A DRP compares two time series with $\approx 5\,\mathrm{K}$ temperature difference, either *both without defect*, or the *first without* and the *second with defect*.
  To do the latter, the first measurement is taken out of the *no defect* measurement series and the second out of the *defect measurement* series. These two compared measurements were thus in reality not taken several minutes after each other, but indeed on different days. We consider the temperature difference here the most important difference.
- The aim is to find a feature out of the DRPs that has great differences in value for *no defect – defect* time series compared to *no defect – no defect* time series.
- We decided to investigate merely RR out of DRPs, i.e., the portion of recurrence points to all points of a plot (pre-investigations showed that RR suffices).

We choose RQA parameters – embedding dimension, delay, and recurrence threshold – in a data driven way [26–28], i.e., we look for the parameter set that serves our goal best (instead of determining the parameters beforehand). A training-test approach is

applied: best parameters are determined on one data set and these parameters are applied (i.e., tested) on a different data set. The training data set are the signals of transducer path T1–T7 without and with defect D24, for test we use the transducer path T6–T12 without and with defect D04 (Fig. 7).

For training we choose 10 K steps of temperatures ascending and descending once between ≈ 20 °C and ≈ 50 °C (Fig. 9). The lower amount of time series saves computational cost for training.

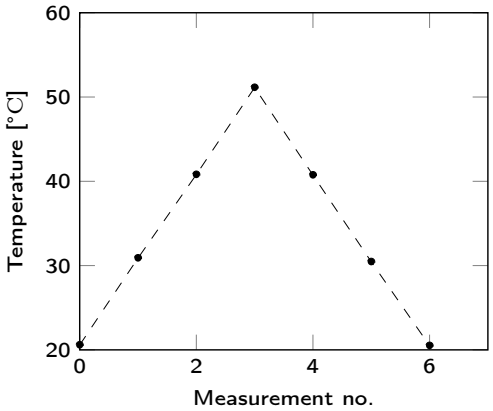

Fig. 9. Temperatures used for training (determination of RQA parameters); difference recurrence plots are computed between time series taken at subsequent temperatures (either both without defect or the first without and the second with defect).

DRPs are computed for 12 (two times six) time series pairs: time series no. 0 and 1, 1 and 2, and so on (Fig. 9), each of the second time series either without or with defect. Out of these DRPs, $m = 6$ RR_b values are computed for *no defect – no defect* pairs and $m = 6$ RR_d for *no defect – defect* pairs. Results are defined to be best if the following maximum is reached

$$\max_{l=1\ldots L} \left(\left| \frac{\sum (RR_b - RR_d)}{m} \right| - 3\sigma_b \right) \tag{7}$$

over L parameter sets. The L parameter sets result from the chosen variation of the (in this case, for the feature recurrence rate) three RQA parameters, see below. RR for each combination of parameters is computed and the parameter set chosen, for which maximum Eq. (7) is achieved. The RR of DRPs *no defect – defect* shall differ as much as possible from those of DRPs *no defect – no defect*. The standard deviation σ_b of the six RR values for *no defect – no defect* is a penalty and must not be too high. If σ_b were too high, the individual values of RR_b would vary and it would be difficult to find a common threshold to distinguish between whether or not a defect occurred, though the individual differences between RR_b and RR_d might be high. In empirical trials a weighting of 3 of σ_b turned out to deliver good results.

We determine the maximum of Eq. (7) over a wide range of the RQA parameters:

- The recurrence threshold ε is varied in a way that RR of almost 0 and almost 1 is achieved.
- With a mean frequency of the sending pulse of 40 kHz and a digitisation frequency of 10 MHz, one period is covered by approximately 250 data points. Initially, a maximum delay of 200 (corresponding to 0.02 ms) has been chosen to cover clearly

more than half a period. A step of 20 (corresponding to 0.002 ms; less than one tenth of a period) is considered sufficient.
– Embedding dimension has initially been varied from 1 to 20 (in steps of 1).

When computing the maximum, Eq. (7), it turns out that embedding dimension and delay reach their maxima $d = 20$ and $\tau = 200$ (corresponding to 0.02 ms). An increase of delay to 260 still showed $\tau = 200$ as optimum. An increase of embedding dimension to 30 and finally to 40 revealed that $d = 40$ indeed delivers best results. No further increase of the embedding dimension is investigated due to the short length of the embedded time series (cf. Sect. 4.2).

Thus $d = 40$ and $\tau = 200$ are identified as optimum embedding parameters; in addition, an optimum recurrence threshold of $\varepsilon = 0.3$ is determined.

4.2 Evaluation (test) results

We have determined the optimum RQA parameters for the feature RR out of DRPs in a training like manner at time series of transducer path T1–T7 without and with defect D24.

Evaluation (test) is now performed at guided ultrasonic wave signals of transducer path T6–T12 without and with defect D04 (Fig. 7).

For benchmark, we start with the simple feature maximum of each time series [3]. Time series out of two cycles of ascending and descending temperatures are taken and for one temperature step in this cycle the defect D04 is introduced, e.g., at ≈ 21 °C (Fig. 10). In reality, for our investigations we take the time series up to — for this example — 21 °C out of the data of no defect measurements and the time series from ≈ 26 °C on out of the data of measurements with defect D04 present.

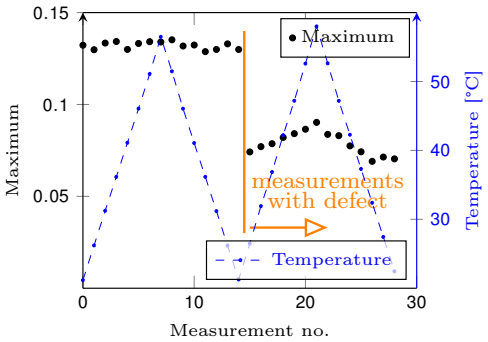

Fig. 10. Feature maximum out of time series at different temperatures without defect up to ≈ 21 °C and with defect D04 from ≈ 26 °C on. The maximum clearly decreases once a defect occurs.

For continuous baseline update, we want to compare a current measurement with a previous one (the baseline). Thus, we calculate the percentaged change between the feature, here the maximum, of two subsequent measurements up to the point when the defect occurs. Following the nomenclature in [3], we use signal discrepancy, SD, for a percentaged change in the following.

To remind about the continuous baseline update, as long as only small changes between two subsequent measurements occur, the current measurement becomes the new baseline. Once the first large signal discrepancy (percentaged change) occurs (here: the maximum clearly decreases), the previous measurement is kept as baseline.

Thus, for all measurements above ≈ 26 °C (right of the vertical line in Fig. 11) the signal discrepancy SD is computed between the last time series without defect — the baseline — and the current measurement. This way, the SDs stay large (Fig. 11, right of the vertical line).

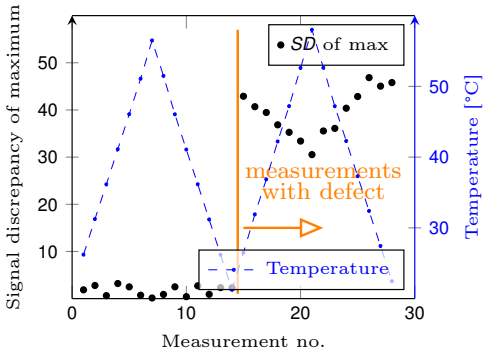

Fig. 11. Signal discrepancy (percentaged change) between time series maxima at different temperatures without defect up to ≈ 21 °C and with defect D04 from ≈ 26 °C on. The maximum clearly increases once a defect occurs.

The signal discrepancies for on one hand *no defect – no defect* and on the other hand *no defect – defect* are clearly different: already this very simple feature shows the occurrence of a defect.

Maack et al. [3] showed that RR out of standard, univariate RPs outperforms the feature maximum. RQA parameters were determined similarly to the way described in Subsect. 4.1; Eq. (7) to find the optimum parameters was also applied, only the used RRs were those of single RPs (without and with defect). Signal discrepancies were computed in the same way as for the feature maximum (Fig. 12).

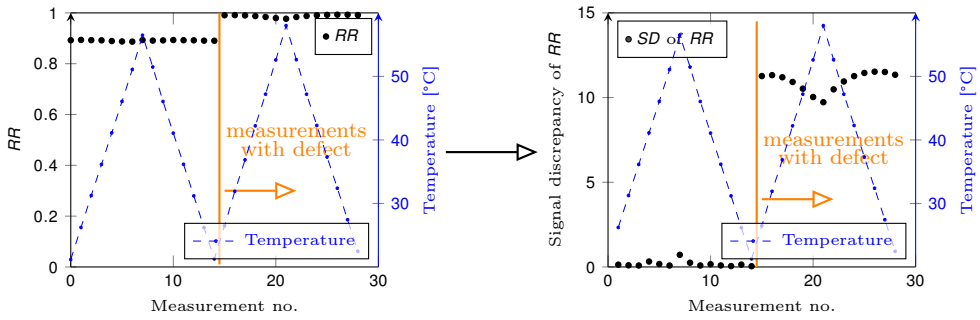

Fig. 12. Recurrence rate per time series at different temperatures without defect up to ≈ 21 °C and with defect D04 from ≈ 26 °C on (left) and signal discrepancies between each pair of subsequent *RR* (right).

The signal discrepancy from *no defect* to *defect* is higher for the feature maximum than for RR (Fig. 11 vs. 12, first value right of the vertical line). However, the proportion of this value to the maximum signal discrepancy between two subsequent time series *no defect – no defect* (left of the vertical line in Figs. 11 and 12) is crucial: this is the basis for setting a threshold to distinguish between *no defect – no defect* and *no*

defect – *defect* time series, i.e., for detecting defects. This proportion is — for defect occurrence at this temperature jump — slightly better for RRs from single RPs than for the feature maximum.

The results above, taken from [3], handle features taken per time series and its signal discrepancies to compare two time series. This study treats results of RR of DRPs as bivariate feature, which directly compares two time series. These have been computed on two subsequent time series of transducer path T6 – T12 of the same 30 varying temperature (Fig. 8) time series for which maximum and single RP RRs have been computed above. Defect D04 was introduced at temperature 26 °C.

The training has been used to find RQA parameters that lead to the largest difference of RRs between DRPs of *no defect* – *no defect* time series on one hand and *no defect* – *defect* time series on the other hand, both with temperature differences of ≈ 10 K (Subsect. 4.1).

With these parameters, the distance plots of two *no defect* – *no defect* time series of transducer pair T6 – T12 are so similar (Fig. 13) that its difference (Fig. 14 left hand side) is smaller than the determined recurrence threshold; RR is almost 1 (Fig. 14 right hand side). We have chosen here the temperature step from ≈ 46 °C to ≈ 51 °C, which leads to the lowest RR of 0.998; for all other investigated temperature steps, $RR > 0.999$. In this evaluation, the temperature has, thus, practically no influence on the time series.

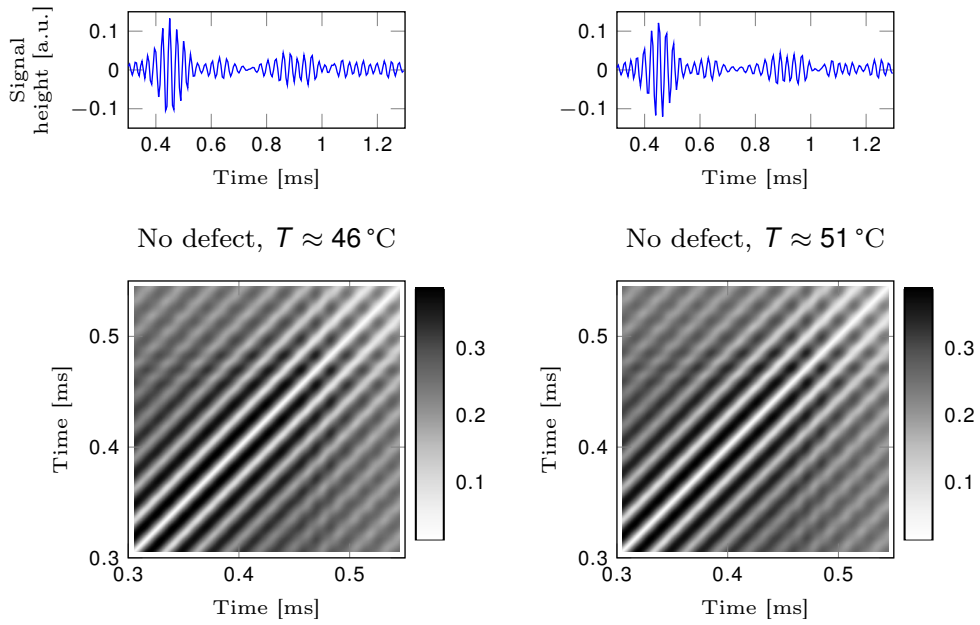

Fig. 13. Time series and according distance plots both without defect at temperatures ≈ 46 °C and ≈ 51 °C.

The situation changes completely when comparing distance plots of time series *no defect* – *defect* for a temperature step of ≈ 5 K, here our standard example of a measurement at ≈ 21 °C without defect and a measurement at ≈ 26 °C with defect (Fig. 15). The resulting DRP (Fig. 16, left hand side) contains much larger differences than the one for *no defect* – *no defect* (Fig. 13, left, same scale used). The resulting DRP (Fig. 16, right hand side) shows an RR smaller than 0.2; the differences of the

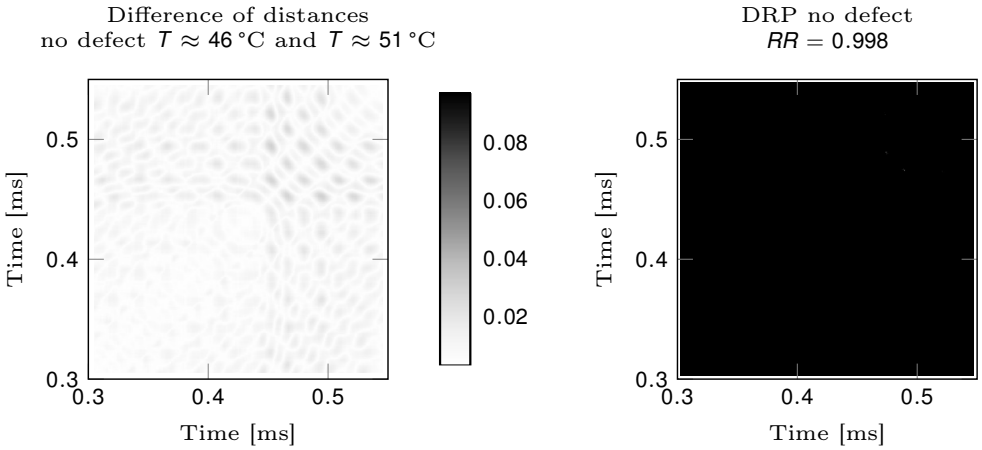

Fig. 14. Difference of distances (left) and its thresholded version (DRP) of two time series measured without defect at $\approx 46\,°C$ and $\approx 51\,°C$.

distances are relatively large except for the last half tenth of a micro second or so. Note that the embedded time series are small (0.22 ms) compared to the original time series (1 ms) due to the large embedding dimension $d = 40$.

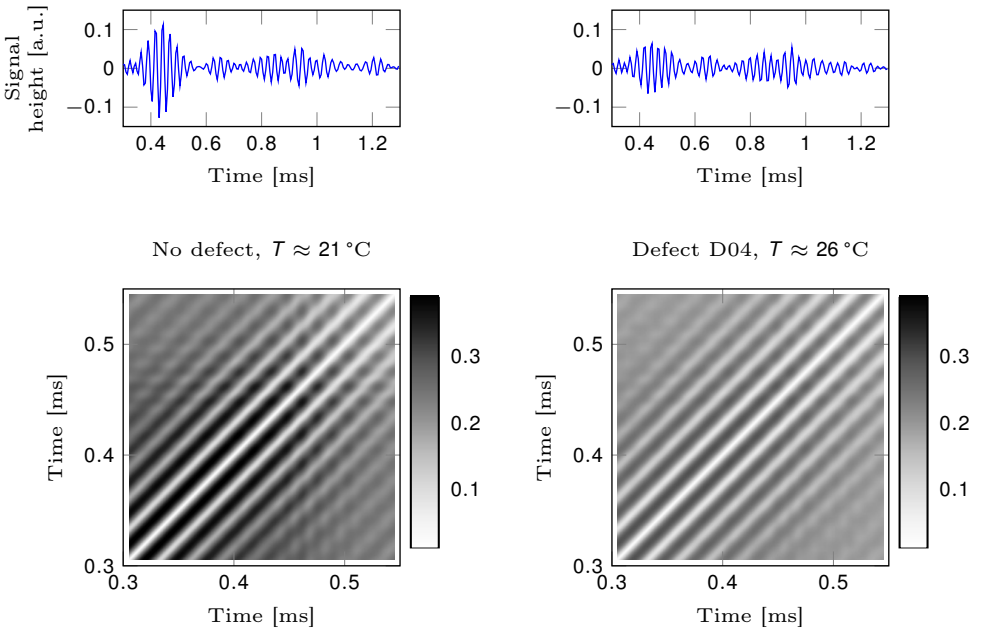

Fig. 15. Time series and according distance plots without defect at $\approx 21\,°C$ and with defect at $\approx 26\,°C$.

This massive reduction of the RR decreases a bit when comparing measurements with defects at further temperatures to the measurement without defect at 21 °C (the baseline) (Fig. 17, RR values right of the vertical line).

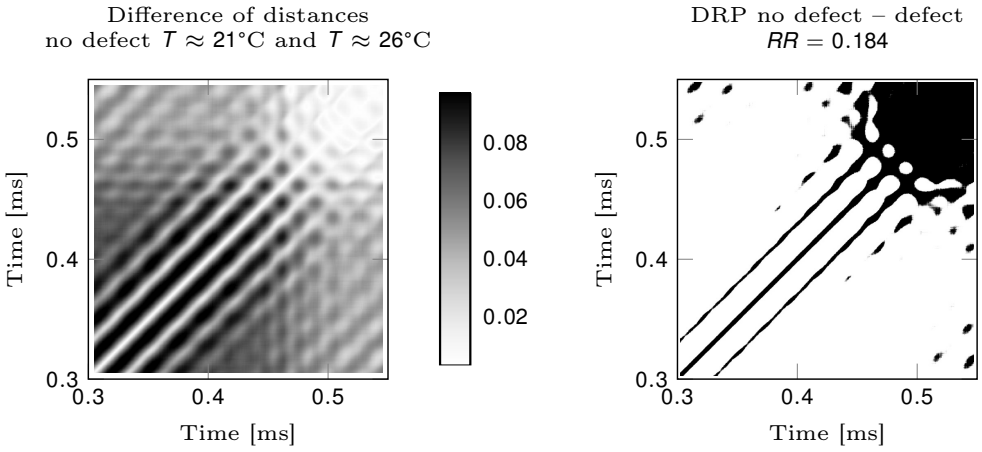

Fig. 16. Difference of distances (left) and its thresholded version (the difference recurrence plot) of a time series measured without defect at ≈ 21 °C and one with defect at ≈ 26 °C.

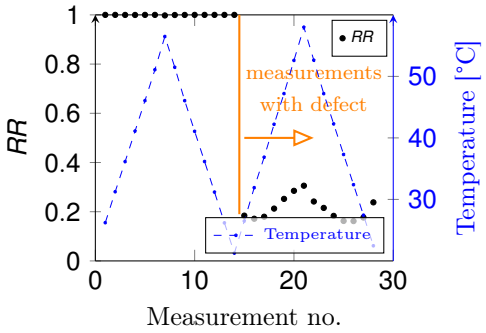

Fig. 17. Recurrence rate of DRPs between time series at different temperatures without defect up to ≈ 21 °C and with defect D04 from ≈ 26 °C on. Massive decrease of *RR* once a defect occurs.

We use next the difference of the RR to full recurrence, $1 - RR$ (Fig. 18), to get a presentation more similar to that of the signal discrepancies of univariate features maximum or RR from standard RP. The maximum of $1 - RR$ for *no defect – no defect* time series is 0.23%, the value for the first change from *no defect* to *defect* is 81.6%. This is clearly better than the signal discrepancies for feature maximum (Fig. 11) and *RR* from standard RPs (Fig. 12 right).

Going one step further, we are looking now at other temperature steps than from ≈ 21 °C to ≈ 26 °C for the first appearance of the defect. Again, it is important to compare

- the signal discrepancy for the last measurement without defect and the first measurement with defect at an ≈ 5 K temperature difference of the features maximum as well as standard RP recurrence rate with
- the maximum signal discrepancy between the features of two subsequent time series (≈ 5 K temperature difference), both without defect.

Similarly, for DRPs, we compare

- RR of a DRP of the last measurement without defect and the first measurement with defect, ≈ 5 K temperature difference with

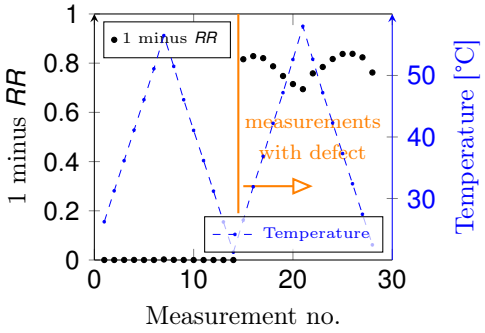

Fig. 18. 1 minus recurrence rate of DRPs between time series at different temperatures without defect up to ≈ 21 °C and with defect D04 from ≈ 26 °C on.

– the maximum RR of a DRP of two subsequent measurements without defect (≈ 5 K temperature difference).

We do these comparisons for the temperature steps from ≈ 21 °C to ≈ 26 °C, ≈ 31 °C to ≈ 36 °C, ≈ 41 °C to ≈ 46 °C, ≈ 51 °C to ≈ 41 °C, ≈ 41 °C to ≈ 31 °C and ≈ 31 °C to ≈ 21 °C, thus also on descending temperatures (cf. Fig. 8).

Signal discrepancies of features maximum and RR of standard RPs show similar performance (Fig. 19 and 20). The scales in the figures are different, but the key value is the ratio between the signal discrepancies of *no defect – defect* and *no defect – no defect*, which can be seen to be similar.

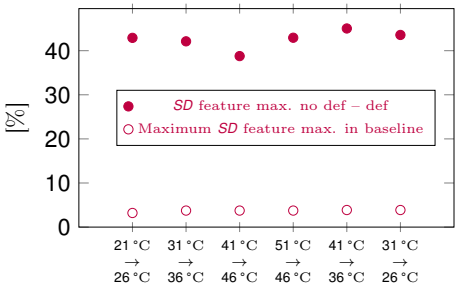

Fig. 19. Signal discrepancies between feature maximum of two subsequent time series (≈ 5 K temperature change): maximum of signal discrepancy of all subsequent time series both without defect (smaller values, empty circles) and signal discrepancy between the last measurement without defect and the first measurement with defect (greater values, filled circles; temperatures given at the horizontal axis).

The situation massively improves for $1 - RR$ for DRPs (Fig 21).

A summarising comparison can be achieved directly with the ratio

$$\frac{SD_{\text{nodef}} - SD_{\text{def}}}{SD_{\text{nodef}} - SD_{\text{nodef}}} \tag{8}$$

of feature maximum and RR of standard RPs, respectively, and

$$\frac{RR_{\text{nodef-def}}}{RR_{\text{nodef-nodef}}} \tag{9}$$

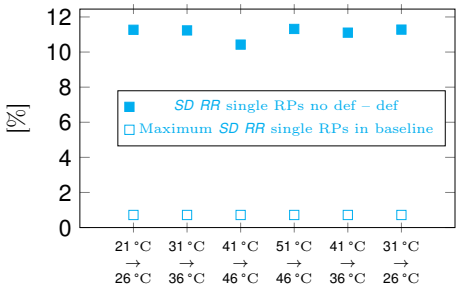

Fig. 20. Signal discrepancies between recurrence rate of standard RPs of two subsequent time series ($\approx$ 5 K temperature change): maximum of signal discrepancy of all subsequent time series both without defect (smaller values, empty squares) and signal discrepancy between the last measurement without defect and the first measurement with defect (greater values, filled squares; temperatures given at the horizontal axis).

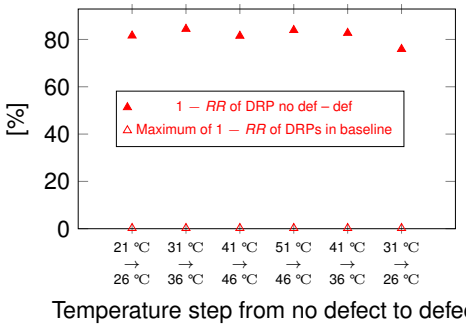

Fig. 21. Recurrence rate of difference RPs of two subsequent time series ($\approx$ 5 K temperature change): maximum of $1 - RR$ of all subsequent time series both without defect (smaller values, empty triangles) and $1 - RR$ of DRP between the last measurement without defect and the first measurement with defect (greater values, filled triangles; temperatures given at the horizontal axis).

of DRPs (Fig. 22). The very slight improvement through RR of standard RPs compared to feature maximum can still be seen; remarkable is, however, the hugely improved ratio for RR of DRPs, which is between 300 and 400, compared to values between 10 and 20 for standard RP RR and feature maximum (Fig. 22).

DRPs have thus shown for this application that they are a useful means to differentiate between two kinds of small differences between time series. In this application — damage detection in a composite plate using guided ultrasonic waves — they can clearly separate between on one hand differences between time series of two measurements both without defect but with temperature difference and, on the other hand, between time series of a measurement without defect and one measurement with defect and temperature difference. So, DRPs help for this application to distinguish damages from temperature differences.

5 Conclusion

Specific research questions require modifications in the RP approach. When interested in studying small differences between time series, the well-known approaches of RP

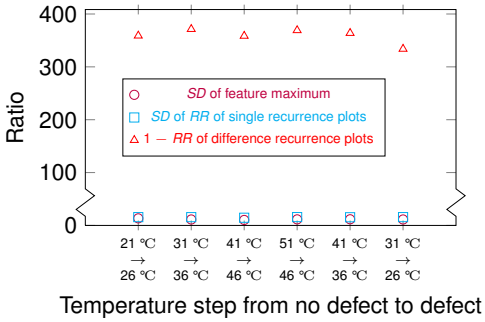

Fig. 22. Ratios between signal discrepancies *no defect – defect* and maximum signal discrepancy *no defect – no defect* for features maximum and RR of standard RPs, and ratio between RR of difference RPs *no defect – defect* and *no defect – no defect* (maximum value for the latter). Ratios for RR of standard RPs very slightly, ratios of RR of DRPs hugely better than for feature maximum.

based coupling analyses are not suitable, because they are too sensitive to identify smallest similarities or couplings. Our novel approach based on RPs of differences in the signals' distance matrices enables us to detect such small deviations. In this study, we have demonstrated the potential of this difference RP (DRP) by studying the increasing deviations within a prototypical model system which is slightly disturbed by a small systematic external signal. Compared to standard approaches (Pearson correlation, power spectra, wavelet, cross and joint recurrence analyses), the DRP approach was superior in detecting such small distortions in a static test model and also during continuously increasing deviations.

The reason for this better performance is the tailored design of the new distance measure used in the RP. Instead of testing the null-hypothesis that the systems are not linked to each other, the null-hypothesis is that the systems are identical. For such a test, all deviations in the geometry of the phase space trajectories are used (i.e., also differences of far away states and not only states in the neighbourhood of the reference state). Alternative measures for testing the modified hypothesis could be applied and compared in future analysis.

The application of this novel approach for structural health monitoring using guided ultrasonic waves is promising. Guided ultrasonic waves can be used to detect damages, in this example in a composite plate. The challenge is to distinguish damages from the effect that varying temperature has. We show that RP parameters can be chosen such that

- DRPs have a very high recurrence when they derive from two time series coming from measurements at different temperatures, but both without damage,
- DRPs have a largely reduced recurrence when they derive from one time series from a measurement without defect and from one time series from a measurement with defect and at different temperature.

The novel DRPs approach has practical applications in engineering and other fields where the detection of slight differences are used for diagnostic purposes.

6 Data and Code Availability

Matlab Code for computations in chapter 3 and Python Code for RQA computations in chapter 4 can be found at Zenodo DOI:10.5281/zenodo.7229221.

References

1. Abbas Fahr. *Aeronautical Applications of Non-destructive Testing.* DEStech Publ., Lancaster, PA, 2014. ID: 865496112.
2. C. Brandt. *Recurrence Quantification Compared to Fourier Analysis for Ultrasonic Non-Destructive Testing of Carbon Fibre Reinforced Polymers.* Phd thesis, Universität Bremen, 2020.
3. Björn Maack, Carsten Brandt, Michael Koerdt, Christoph Polle, and Axel Siegfried Herrmann. Continuous Baseline Update Using Recurrence Quantification Analysis for Damage Detection with Guided Ultrasonic Waves. *European Physical Journal – Special Topics*, in prep.
4. N. Marwan and J. Kurths. Nonlinear analysis of bivariate data with cross recurrence plots. *Physics Letters A*, 302(5–6):299–307, 2002. doi: 10.1016/S0375-9601(02)01170-2.
5. M. C. Romano, M. Thiel, J. Kurths, I. Z. Kiss, and J. L. Hudson. Detection of synchronization for non-phase-coherent and non-stationary data. *Europhysics Letters*, 71(3):466–472, 2005. doi: 10.1209/epl/i2005-10095-1.
6. M. C. Romano, M. Thiel, J. Kurths, and W. von Bloh. Multivariate Recurrence Plots. *Physics Letters A*, 330(3–4):214–223, 2004. doi: 10.1016/j.physleta.2004.07.066.
7. Y. Hirata and K. Aihara. Identifying hidden common causes from bivariate time series: A method using recurrence plots. *Physical Review E*, 81(1):016203, 2010. doi: 10.1103/PhysRevE.81.016203.
8. J. H. Feldhoff, R. V. Donner, J. F. Donges, N. Marwan, and J. Kurths. Geometric detection of coupling directions by means of inter-system recurrence networks. *Physics Letters A*, 376(46):3504–3513, 2012. doi: 10.1016/j.physleta.2012.10.008.
9. A. Facchini, H. Kantz, and E. B. P. Tiezzi. Recurrence plot analysis of non-stationary data: The understanding of curved patterns. *Physical Review E*, 72:021915, 2005. doi: 10.1103/PhysRevE.72.021915.
10. N. Marwan. How to avoid potential pitfalls in recurrence plot based data analysis. *International Journal of Bifurcation and Chaos*, 21(4):1003–1017, 2011. doi: 10.1142/S0218127411029008.
11. N. Marwan, M. C. Romano, M. Thiel, and J. Kurths. Recurrence Plots for the Analysis of Complex Systems. *Physics Reports*, 438(5–6):237–329, 2007. doi: 10.1016/j.physrep.2006.11.001.
12. K. H. Kraemer, R. V. Donner, J. Heitzig, and N. Marwan. Recurrence threshold selection for obtaining robust recurrence characteristics in different embedding dimensions. *Chaos*, 28(8):085720, 2018. doi: 10.1063/1.5024914.
13. N. Marwan, M. Thiel, and N. R. Nowaczyk. Cross Recurrence Plot Based Synchronization of Time Series. *Nonlinear Processes in Geophysics*, 9(3/4):325–331, 2002. doi: 10.5194/npg-9-325-2002.
14. N. V. Zolotova and D. I. Ponyavin. Phase asynchrony of the north-south sunspot activity. *Astronomy & Astrophysics*, 449(1):L1–L4, 2006. doi: 10.1051/0004-6361:200600013.
15. A. M. T. Ramos, A. Builes-Jaramillo, G. Poveda, B. Goswami, E. E. N. Macau, J. Kurths, and N. Marwan. Recurrence measure of conditional dependence and applications. *Physical Review E*, 95:052206, 2017. doi: 10.1103/PhysRevE.95.052206.
16. M. I. Coco, R. Dale, and F. Keller. Performance in a Collaborative Search Task: The Role of Feedback and Alignment. *Topics in Cognitive Science*, 10(1):55–79, 2018. doi: 10.1111/tops.12300.
17. N. Marwan, Y. Zou, N. Wessel, M. Riedl, and J. Kurths. Estimating coupling directions in the cardio-respiratory system using recurrence properties. *Philo-*

sophical Transactions of the Royal Society A, 371(1997):20110624, 2013. doi: 10.1098/rsta.2011.0624.
18. A. Builes-Jaramillo, N. Marwan, G. Poveda, and J. Kurths. Nonlinear interactions between the Amazon River basin and the Tropical North Atlantic at interannual timescales. *Climate Dynamics*, 50(7–8):2951–2969, 2018. doi: 10.1007/s00382-017-3785-8.
19. J. H. Feldhoff, R. V. Donner, J. F. Donges, N. Marwan, and J. Kurths. Geometric signature of complex synchronisation scenarios. *Europhysics Letters*, 102(3): 30007, 2013. doi: 10.1209/0295-5075/102/30007.
20. T. Takamatsu, K. Yaginuma, and T. Nakajima. Asynchrony estimation of solar irradiance by quantification of joint recurrence plot. pages 692–695, 2019. doi: 10.1109/ICRERA47325.2019.8996732.
21. R. Proulx, P. Côté, and L. Parrott. Use of recurrence analysis to measure the dynamical stability of a multi-species community model. *European Physical Journal – Special Topics*, 164(1):117–126, 2008. doi: 10.1140/epjst/e2008-00838-0.
22. T. Semeraro, R. Buccolieri, M. Vergine, L. De Bellis, A. Luvisi, R. Emmanuel, and N. Marwan. Analysis of the olive groves destructions by xylella fastidosa bacterium effect on the land surface temperature in salento detected using satellite images. *Forests*, 12:1266, 2021. doi: 10.3390/f12091266. Editor's choice article.
23. www.openguidedwaves.de. `http://openguidedwaves.de/`, 2022.
24. Jochen Moll, Jens Kathol, Claus-Peter Fritzen, Maria Moix-Bonet, Marcel Rennoch, Michael Koerdt, Axel S Herrmann, Markus GR Sause, and Martin Bach. Open Guided Waves: online platform for ultrasonic guided wave measurements. *Structural Health Monitoring*, 18(5–6):1903–1914, 2019. doi: 10.1177/1475921718817169.
25. Jochen Moll, Christian Kexel, Serena Pötzsch, Marcel Rennoch, and Axel S. Herrmann. Temperature affected guided wave propagation in a composite plate complementing the Open Guided Waves Platform. *Scientific Data*, 6(1), 2019. doi: 10.1038/s41597-019-0208-1.
26. J. P. Zbilut and C. L. Webber, Jr. Embeddings and delays as derived from quantification of recurrence plots. *Physics Letters A*, 171(3–4):199–203, 1992. doi: 10.1016/0375-9601(92)90426-M.
27. N. Marwan, N. Wessel, U. Meyerfeldt, A. Schirdewan, and J. Kurths. Recurrence Plot Based Measures of Complexity and its Application to Heart Rate Variability Data. *Physical Review E*, 66(2):026702, 2002. doi: 10.1103/PhysRevE.66.026702.
28. S. Schinkel, O. Dimigen, and N. Marwan. Selection of recurrence threshold for signal detection. *European Physical Journal – Special Topics*, 164(1):45–53, 2008. doi: 10.1140/epjst/e2008-00833-5.